Two-Photon Fluorescence Lifetime Imaging of the Skin Stratum Corneum pH Gradient

Kerry M. Hanson,* Martin J. Behne,† Nicholas P. Barry,* Theodora M. Mauro,† Enrico Gratton,* and Robert M. Clegg*

*Laboratory for Fluorescence Dynamics, Department of Physics, University of Illinois, Urbana-Champaign, Illinois 61801, and †Dermatology Service, Veterans Affairs Medical Center and Department of Dermatology, University of California, San Francisco, California 94110 USA

ABSTRACT Two-photon fluorescence lifetime imaging is used to identify microdomains (1–25 μm) of two distinct pH values within the uppermost layer of the epidermis (stratum corneum). The fluorophore used is 2′,7′-bis-(2-carboxyethyl)-5-(and-6)-carboxyfluorescein (BCECF), whose lifetime τ (pH 4.5, $\tau = 2.75$ ns; pH 8.5, $\tau = 3.90$ ns) is pH dependent over the pH range of the stratum corneum (pH 4.5 to pH 7.2). Hairless mice (SKH1-hrBR) are used as a model for human skin. Images ($\leq$50 μm $\times$ 50 μm) are acquired every 1.7 μm from the stratum corneum surface to the first viable layer (stratum granulosum). Acidic microdomains (average pH 6.0) of variable size ($\sim$1 μm in diameter with variable length) are detected within the extracellular matrix of the stratum corneum, whereas the intracellular space of the corneocytes in mid-stratum corneum (25 μm diameter) approaches neutrality (average pH 7.0). The surface is acidic. The average pH of the stratum corneum increases with depth because of a decrease in the ratio of acidic to neutral regions within the stratum corneum. The data definitively show that the stratum corneum acid mantle results from the presence of aqueous acidic pockets within the lipid-rich extracellular matrix.

INTRODUCTION

Within the 10–20 cell layers of the uppermost epidermis (stratum corneum) of human skin, the hydrogen ion concentration decreases 100-1000-fold (Ohman and Vahlquist, 1994). The surface of the skin is acidic, ranging between pH 4.5 and pH 6 depending upon body site, sex, and species, forming what is termed the acid mantle (Dikstein and Zlotogorski, 1994; Ohman and Vahlquist, 1994). In contrast, the first viable epidermal layer (stratum granulosum) below the stratum corneum, $\sim$10 μm below the surface, reaches neutrality. Current research shows that pH greatly influences the barrier nature of the stratum corneum. Thus, understanding both the effect of pH and its origin upon the skin barrier is synonymous with improving topical drug delivery and understanding barrier-influenced diseases like dermatitis and icthyosis. To determine how pH affects barrier function, a method for detecting pH in the stratum corneum on the subcellular level is first needed.

Tape stripping has allowed measurements of pH as a function of stratum corneum depth using a flat electrode (Ohman and Vahlquist, 1994, 1998). These measurements have determined that pH increases with each deeper corneocyte layer showing that a pH gradient exists between the surface and the deepest stratum corneum. There are two drawbacks to tape-stripping measurements. First, it is intrinsically destructive. Once perturbed, the skin naturally undergoes barrier recovery, which may in turn alter the pH of the stratum corneum. Therefore, such measurements do not necessarily measure the pH at equilibrium. Second, using a flat electrode on the stratum corneum provides a bulk measurement of pH over an extended area (square centimeters). The electrode method cannot identify at the subcellular level those compartments, such as the extracellular matrix and/or intracellular spaces, that contribute to the dramatic pH differences observed across the stratum corneum.

Microscopy in conjunction with pH-sensitive fluorescent probes offers a method to determine pH with the required spatial resolution (Hanson et al., 2000). In general, these fluorophores report their local pH through a shift in excitation spectrum and change in the intensity/spectrum of emission as the probe changes between an acid and a base form. These spectral changes are often accompanied by a change in the fluorescence lifetime (Rink et al., 1982; Szmacinski and Lakowicz, 1993). Quantitative use of these probes in a cellular environment presents many challenges. Purely optical absorbance methods for determination of pH are generally not used because of difficulties in measuring the spectrum of a necessarily dilute stain against a complex cellular background absorption. Emission intensity methods have more than adequate sensitivity of detection for probe concentrations thought not to disturb normal cell behavior; however, because of inhomogeneous labeling, simple intensity measurements cannot be used to determine pH in the cellular environment. In such cases, either excitation ratio or emission ratio methods can be used. For lamp-based systems it is possible to rapidly change excitation filters to facilitate ratio imaging of samples that are not opaque.

Submitted January 8, 2002, and accepted for publication May 1, 2002.

K.M.H. and N.P.B. contributed equally to this work.

Address reprint requests to Dr. Kerry M. Hanson, Laboratory for Fluorescence Dynamics, University of Illinois, 1110 W. Green Street, Urbana, IL 61801. Tel.: 217-244-5620; Fax: 217-244-7187; E-mail: khanson@uiuc.edu.

0006-3495/02/09/1682/09 $2.00

In this work, three-dimensional information upon skin with subcellular resolution is desired. This suggests the use of confocal microscopy techniques. In this case, the availability of suitable laser lines poses a difficulty. In addition, it is difficult to change between laser lines rapidly, and it is difficult to retain the exact depth of focus of the different excitation wavelengths. These problems make excitation ratiometric methods cumbersome and unattractive. Emission ratio methods are also possible in the case of acquiring data within the relatively thin (~15 μm) stratum corneum. However, for thicker samples, quantification using emission ratio imaging is complicated by wavelength-dependent inhomogeneous absorption and scattering as the fluorescence light leaves the skin sample in its path to the detector (Jacques, 1996). More specifically in the case of measuring pH within the stratum corneum, a single probe is not commercially available to date to detect pH over the pH range of the stratum corneum by emission ratio methods. Multiple probes would be required to determine pH by this method within the stratum corneum.

Fluorescence lifetime imaging offers a solution to these problems and is compatible with confocal microscopy. The lifetime is independent of probe concentration and inhomogeneities in excitation and emission light paths. Scatter will delay the emitted light in reaching the detector, but this effect is negligible (picoseconds) compared with typical fluorescence lifetimes (nanoseconds) for the tissue penetration in this study.

When working with bulk tissue, the penetration of the excitation light must be considered. Two-photon excitation using near-infrared light and without a confocal pinhole in the emission path has been shown to allow sectioned imaging at greater depths into a tissue sample compared with ultraviolet confocal excitation (Masters et al., 1997). Because in two-photon microscopy no pinhole is used, subsequent scatter of the fluorescent emission does not result in rejection by the confocal pinhole as in one-photon excitation.

A number of fluorescein-derived dyes are available for measurement at near physiological pH. For this work we have chosen to use 2′,7′-bis-(2-carboxyethyl)-5-(and-6)-carboxyfluorescein (BCECF) with a pK_a of 7.0 (Rink et al., 1982; Szmacinski and Lakowicz, 1993; Haughland, 1998). The emission from BCECF has a maximum at 535 nm. The broad tuning range of the mode-locked Ti:sapphire laser used in this study allows selection of an excitation wavelength that minimizes contributions from autofluorescence.

MATERIALS AND METHODS

Materials

BCECF (Fig. 1) was purchased and used without further purification from Molecular Probes (Eugene, OR). Solutions of BCECF (10 μM) are made in PBS or citric acid buffers (10 mM plus 3 mM KCl plus 140 mM NaCl). The pH is adjusted between pH 2 and pH 12. Chloral hydrate (12.5 mg in 0.25 ml of sterile water) is supplied by the Division of Animal Resources (University of Illinois, Urbana-Champaign).

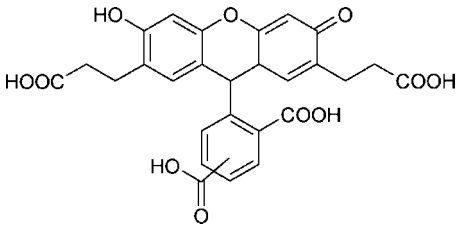

FIGURE 1 The molecular structure of BCECF.

Animals

Hairless mice (Crl:SKH1-hrBR) were obtained from Charles River Laboratories (Wilmington, MA). Animals were fed Purina mouse diet and water ad libitum. Animals were 8–12 weeks old at the time of the experiments. The experiments were done with the University of Illinois' Division of Animal Resources approval (01087).

Skin samples

The animal was anesthetized with chloral hydrate, and 50–100 μl of BCECF (50 μM in ethanol) was applied to a small region (~0.25 cm^2) on the back skin of the animal. Aqueous solutions of BCECF were not used as they are excluded from the stratum corneum or would require a much longer incubation time than the ethanol-based solution. Three applications of BCECF were made to the same region within 45 min for a total incubation time of 1 h. The animal was sacrificed, and the BCECF-incubated skin was removed. An additional piece of skin that had no dye applied to it was removed for control experiments.

Two-photon fluorescence lifetime imaging microscope

The instrument has been described in detail (Fig. 2) (So et al., 1996; Hanson et al., 2000). A titanium:sapphire laser system (Millenia-pumped Tsunami, Spectra-Physics, Mountain View, CA) was used as the two-photon excitation source. Two-photon excitation of the sample was achieved by coupling the 820-nm output (<1 mW at the sample) of the laser through the epifluorescence port of a Zeiss Axiovert microscope (Maple Grove, MN). The excitation beam was diverted to the sample by a dichroic filter (Q560LP, Chroma Technologies), and the fluorescence emission was collected using a Hamamatsu (R3996, Bridgewater, NJ) photomultiplier Filters (BG39 and HG525/50M, Chroma Technologies, Brattleboro, VT) were placed in the fluorescence emission path to block scattered IR and pass BCECF fluorescence. Scanning mirrors and ×40 infinity corrected oil objective (Zeiss F Fluar, 1.3 N.A.) were used to image areas between 625 and 4000 μm^2. Depth z-slices are obtained by adjusting the objective focus with a motorized driver (ASI Multi-Scan 4, Lexington, KY).

Fluorescence lifetime data were acquired using the heterodyne frequency-modulation method (Jameson et al., 1984; Alcala et al., 1985). In this method, the phase and modulation of the high-frequency fluorescence emission are detected relative to the phase and modulation of the high-frequency repetitive light source. In our experiments, the sample fluorescence was excited by a $Ti:Al_2O_3$ laser whose frequency spectrum of the pulse train is 80 MHz. The fundamental harmonic of the BCECF fluorescence was measured using heterodyning methods. The decay of the BCECF fluorescence was monoexponential at each pH extreme (Szmacinski and Lakowicz, 1993). A frequency synthesizer (PTS 510, Precision Test Sources, Littleton, MA), which is phase-

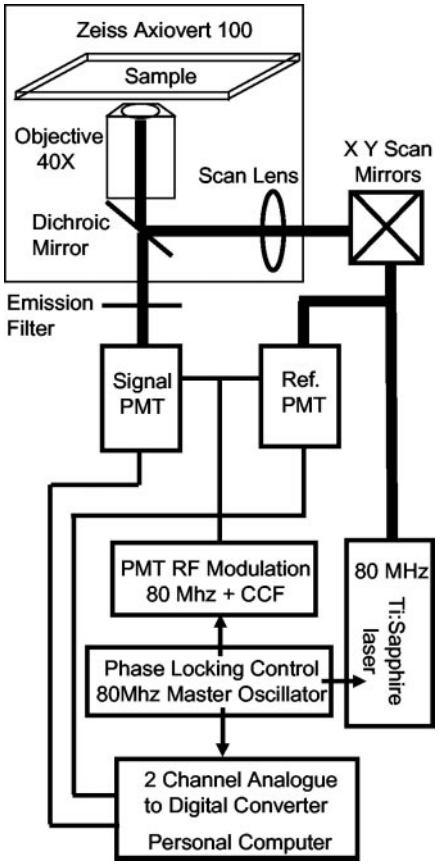

FIGURE 2 Experimental diagram of the two-photon fluorescence lifetime imaging instrument.

locked to the repetition frequency of the laser, drives a RF power amplifier (2 W, M502, Rf Power Labs) that is used for modulating the amplification of the detector photomultiplier (PMT, R3996, Hamamatsu) at the master frequency plus an additional cross-correlation frequency (2.5 kHz). A beam-splitter in the light path outside the microscope diverted 4% of the fundamental to a reference PMT (R928, Hamamatsu). The reference PMT was modulated identically to that of the detector PMT. This allowed for correction of phase and amplitude noise in the excitation beam. The photocurrent output from both PMTs was digitized using a plug-in analog-to-digital card (DRA Laboratories, Sarasota, FL). The differential phase between the excitation signal and the fluorescence signal was determined using a fast Fourier transform algorithm to analyze each individual signal. We sampled at eight equally spaced times during each period of the cross-correlation (50 μs per time point) to determine the phase delay, modulation, and average intensity at each pixel. An image is composed of 256×256 pixels.

Data analysis

Frequency-domain lifetime data acquisition has been described in detail (Jameson et al., 1984; Alcala et al., 1985). The lifetime of the fluorophore was determined by the phase delay (ϕ) and the relative modulation (M) between the fluorescence signal and the sinusoidally modulated excitation light at frequency ν ($\omega = 2\pi\nu$). The phase delay and modulation are defined as

$$\phi = \tan^{-1}\frac{S}{G} \tag{1}$$

$$M = (S^2 + G^2)^{1/2} \tag{2}$$

TABLE 1 Calibration of solution-phase BDECF after excitation at 820 nm

	Fluorescence intensity (λ_{ex} = 820 nm)	pH	τ_{phs}	τ_{mod}	Average τ
HBCECF	348.5	4.5	2.72 (0.04)	2.78 (0.02)	2.75
$BCECF^-$	59.5	8.5	3.93 (0.08)	3.87 (0.04)	3.90

G and S are described by functions of both the lifetime (τ_i) and the contribution to the overall intensity (fractional intensity, f_i) of each fluorescent species i.

$$G = \sum_i \frac{f_i}{1 + \omega^2\tau_i^2} \tag{3}$$

$$S = \sum_i f_i \frac{\tilde{\omega}\tau_i}{1 + \omega^2\tau_i^2} \tag{4}$$

$$\sum_i f_i = 1 \tag{5}$$

If the intrinsic lifetime τ_n is the same for each species, then the fluorescence quantum yield (ϕ_i) of a molecule in each of its different configurations is proportional to τ_i and the molar or species ratio (R_m) of the species fractions F_i is described by

$$R_m = \frac{F_1}{F_2} = \frac{\tau_2}{\tau_1}\frac{f_1}{f_2}, \tag{6}$$

where, f_i, τ_i, and the emission intensities increase (or decrease) by the same factor (Jameson et al., 1984). For molecules like BCECF (Fig. 1), τ_n differs between the protonated and deprotonated form. As a result, the fluorescence intensity between the two forms of BCECF increases by a factor of ~6 between pH 4.5 and pH 7.5, unlike τ_i, which changes by a factor of 1.4 (Table 1). Therefore we cannot use the expression in Eq. 6. Instead, the species fractions of BCECF, F_i, is calculated by accounting for the change in intensity between the two configurations of BCECF where

$$F_i = \frac{f_i}{I_i} \tag{7}$$

I_i is the relative fluorescence intensity of either protonated BCECF or $BCECF^-$ following two-photon excitation at 820 nm ($I_{BCECF^-} = 5.9$; $I_{HBCECF} = 1$). This procedure fits the time-resolved frequency data (phase and modulation) to extract the f_i (or F_i) values; the fluorescence lifetimes of $BCECF^-$ and HBCECF are known and kept constant during the fit. This is a linear fitting procedure (Clegg and Schneider, 1996; Lakowicz, 1999).

Lifetime measurements were acquired relative to a reference sample to account for instrumentation effects. The true phase ϕ_t and modulation M_t values for a fluorophore are described by

$$\phi_t = C_\phi \pm \phi_r \tag{8}$$

$$M_t = C_M M_r \tag{9}$$

$C_{\phi,M}$ are correction factors that account for instrumentation effects upon the measurements, and t and r indicate the true and measured values of the phase and modulation, respectively.

Fluorescein (pH 10, 5 μM) was used as the reference (τ = 4.05 ns) for lifetime-resolved data collected on BCECF both in solution and in the skin.

Correcting the lifetime-resolved data for the skin's index of refraction

In addition to instrumentation effects, lifetime measurements of BCECF were corrected for differences in the index of refraction (η) between the solution phase and skin environments. The fluorescence lifetime τ of BCECF is influenced by the index of refraction of the surrounding environment, such that τ of BCECF in skin differs from τ of BCECF in aqueous solution (see Eq. 15) by

$$\tau \propto \eta^{-2} \tag{10}$$

The $\eta_{water} = 1.33$ and $\eta_{skin} = 1.37–1.39$ (Knuttel and Boehlau-Godau, 2000). Thus, τ of a fluorophore in skin is 0.9τ of that fluorophore in solution. This is confirmed (see discussion of Eq.15) by a comparison between the lifetime-resolved data of fluorescein in solution and in mouse skin (skin incubated with 50-μm fluorescein) ($\tau_{solution} = 4.05$ ns; $\tau_{skin} = 3.73$ ns). The difference in the solution phase and skin τ values corresponds to correction factors of $C_\phi = 5^0$ and C_M of 1.2 (Eqs. 8 and 9) that account for the difference in η.

Calculating pH

Given that

$$HBCECF \xrightarrow{K_a} H^+ + BCECF^-,$$

the acid dissociation constant for this reaction (K_a) is defined by the ratio of the concentrations of the reactants and products:

$$K_a = \frac{[H^+][BCECF^-]}{[HBCECF]} \tag{11}$$

Solving for $[H^+]$ yields the Henderson-Hasselbach equation where

$$pH = pK_a + \log \frac{[BCECF^-]}{[HBCECF]} \tag{12}$$

The pK_a of BCECF is 7.0 ((Rink et al., 1982; Szmacinski and Lakowicz, 1993; Haughland, 1998), Fig. 3 *b*). In this experiment, [HBCECF] and $[BCECF^-]$ are equivalent to the number of molecules, or the species fraction of molecules F_i, with the *i*th lifetime component in the protonated and unprotonated configurations of BCECF, respectively. Thus,

$$pH = pK_a = \log \frac{F_{BCECF^-}}{F_{HBCECF}} \tag{13}$$

RESULTS AND DISCUSSION

Determination of τ_{HBCECF} and τ_{BCECF^-}

BCECF (Fig. 1) exists in one of two possible molecular configurations. At acidic pH BCECF is protonated (HBCECF), and at basic pH it is unprotonated ($BCECF^-$). At a pH in which more than one protonation state of BCECF exists (pH 5 < solution pH < pH 8 (Haughland, 1998)), the species fractions F_{HBCECF} and F_{BCECF^-} represent the fraction of molecules with the lifetime components τ_{HBCECF} and τ_{BCECF^-}, respectively (Eqs. 1–7). Thus, to calculate F_{HBCECF} and F_{BCECF^-} values in the skin (and therefore pH (Eqs. 12–13)), τ_{HBCECF} and τ_{BCECF^-} are determined first under identical experimental conditions as those used to determine pH in the heterogeneous environment of the skin.

Fig. 3 *a* shows the phase delay and modulation data of solution-phase BCECF at different solution pH. The data points in Fig. 3 *a* are calculated from the fractional intensities of the two forms of BCECF, and thus the data curves are weighted to the acidic side of the *x* axis (see Materials and Methods). Fig. 3 *b* displays the species fraction of $BCECF^-$ at different solution pH and shows that the experimental pK_a is 6.87, which agrees with the literature value (Rink et al., 1982). The phase and modulation data are used to calculate the values of τ_{phase} and τ_{mod}, respectively, at each pH, which are averaged and displayed in Fig. 3 *c*. Using the data in Fig. 3, τ_{phase} and τ_{mod} are calculated for the two electronic states of BCECF (HBCECF and $BCECF^-$, Table 1). The shortest lifetime is achieved at low pH when BCECF is in its acidic form, and the longest lifetime is achieved at higher pH when BCECF is fully unprotonated. The difference in τ_i is 1.4-fold (Table 1), unlike the fluorescence intensity between the two forms of BCECF, which increases by ~5.9 times between pH 4.5 and pH 7.5. This characteristic reflects that τ_i is not proportional to ϕ_i. The lifetime values determined in our experiment are ~10% less than those reported in the literature (Szmacinski and Lakowicz, 1993). This is a small difference; however, all of our data are internally calibrated with our own measurements.

Comparison of the intensity and lifetime-resolved images

Fluorescence intensity images are compared against both the corresponding modulation and calculated lifetime images of hairless mouse skin incubated with BCECF in Fig. 4. Images are presented for consecutive 1.7-μm depths beginning at the skin's surface until the strata corneum-granulosum junction appears at ~10.2 μm. Because the hairless mouse skin is thinner than human skin, the number of cell layers displayed in Fig. 4 is less than the 10–20 layers (on average) that would be anticipated for human stratum corneum. The images in Fig. 4 show different fells at each depth where the stratum corneum corneocytes have a tightly packed columnar arrangement (MacKenzie, 1969; Christophers, 1971).

As the intensity images show, BCECF clearly concentrates in both the extracellular and intracellular spaces. At the surface, the intracellular space reveals the greatest intensity; however, in the middle corneocyte layers BCECF concentrated more in the lipid-rich extracellular matrix. The average signal intensity from the intercellular space is 100 counts/50 μs, which is significantly above that of the autofluorescence (<4 counts/50 μs) of identical areas. Because the fluorescence intensity of BCECF increases with pH, it can be used to indicate pH in a homogeneous environment. However, because the dye concentration is un-

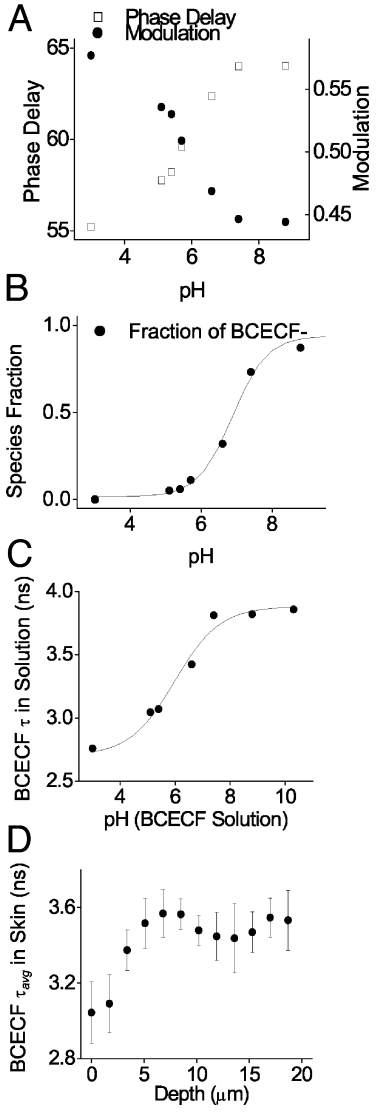

FIGURE 3 Experimental lifetime data of BCECF. (*a*) Measured phase and modulation values of BCECF as a function of solution pH. (*b*) Species fraction of $BCECF^-$, indicating that the pK_a is 6.9. (*c*) Average lifetime τ of BCECF at different solution pH (average of τ_{phs} and τ_{mod}, Table 1). (*d*) τ_{avg} of BCECF detected at different epidermal depths of mouse (Crl:SKH1-hrBR) skin. Each data point in *d* represents the average of images ($\leq 50 \times 50$ μm) taken from two different skin samples. The τ_{avg} values become constant at depths greater than 9 μm where the stratum granulosum appears.

known at individual regions within the skin, simple intensity cannot be used as a direct measurement of pH in our images. A region of bright fluorescence intensity may be an indication of neutral pH, but it may also reflect an area of concentrated dye that yields a large fluorescence signal. Comparing the intensity images with the corresponding modulation and lifetime images (Fig. 4, *b* and *c*) emphasizes this characteristic. Because lifetime measurements are concentration independent, the amplitude variations of the lifetime-resolved images (Fig. 4, *b* and *c*) do not necessarily correlate with the brightness of the fluorescence intensity image (Fig. 4 *a*). This is especially evident in the surface images, where regions of low intensity in the lower left quadrant of the image yield similar modulation and lifetime values as those of the lower right quadrant, which has the greatest intensity. Areas with low modulation have a shorter lifetime and thus are more acidic than those areas corresponding to higher modulation, which correspond to more neutral pH values (Figs. 4 *c* and 3, *a* and *c*).

Correction of the lifetime-resolved data for index of refraction

Lifetime-resolved data are typically acquired relative to a reference standard. A solution of fluorescein was chosen for our experiments because its phase and modulation are not dramatically affected by the pH range of skin. However, unlike solution phase measurements, data acquisition of fluorophores in the heterogeneous environment of the skin warrants an additional correction to be made to the lifetime-resolved data if it is acquired relative to a solution-phase reference standard. This correction is necessary because the skin and solution phase environments affect the absolute value of a fluorophore's τ.

For example, it is true that the τ_i of HBCECF in acidic environments within the stratum corneum is shorter than the τ_i of $BCECF^-$ in the neutral environment of the viable epidermal layers. However, although the relative difference between τ_i of HBCECF and $BCECF^-$ in the skin is identical to the relative difference of the corresponding solution-phase τ values, the absolute τ_i values of HBCECF and $BCECF^-$ in the skin differ from those in solution. For example, averaging the lifetime data over the entire image (τ_{avg}) at each epidermal depth in Fig. 4 *c* reveals that τ_{avg} increases from 3.01 ns at the stratum corneum surface to 3.51 ns in the stratum granulosum and deeper epidermal layers (Fig. 3 *d*). A lifetime of 3.51 ns corresponds to a pH of near 6 (Fig. 3 *c*), which is physiologically improbable as it is well established that the average pH of the viable epidermis is pH 7 (Ohman and Vahlquist, 1994, 1998).

We consider two factors, autofluorescence/scatter and index of refraction, that could account for the 1.1-fold difference in τ_{avg}, and thus the difference in apparent pH, between the solution and skin environments. As the contribution to the overall signal from autofluorescence and scatter increases, thus decreasing the relative contribution from a fluorophore, the detected τ of that fluorophore decreases (Fig. 5). The emission filter and excitation wavelength (820 nm) reduces autofluorescence and scatter of our skin samples to $<1\%$ of the total intensity measured. As Fig. 5 shows, such a low background will not significantly alter the lifetime data of BCECF between the pH 7 solution and skin environments.

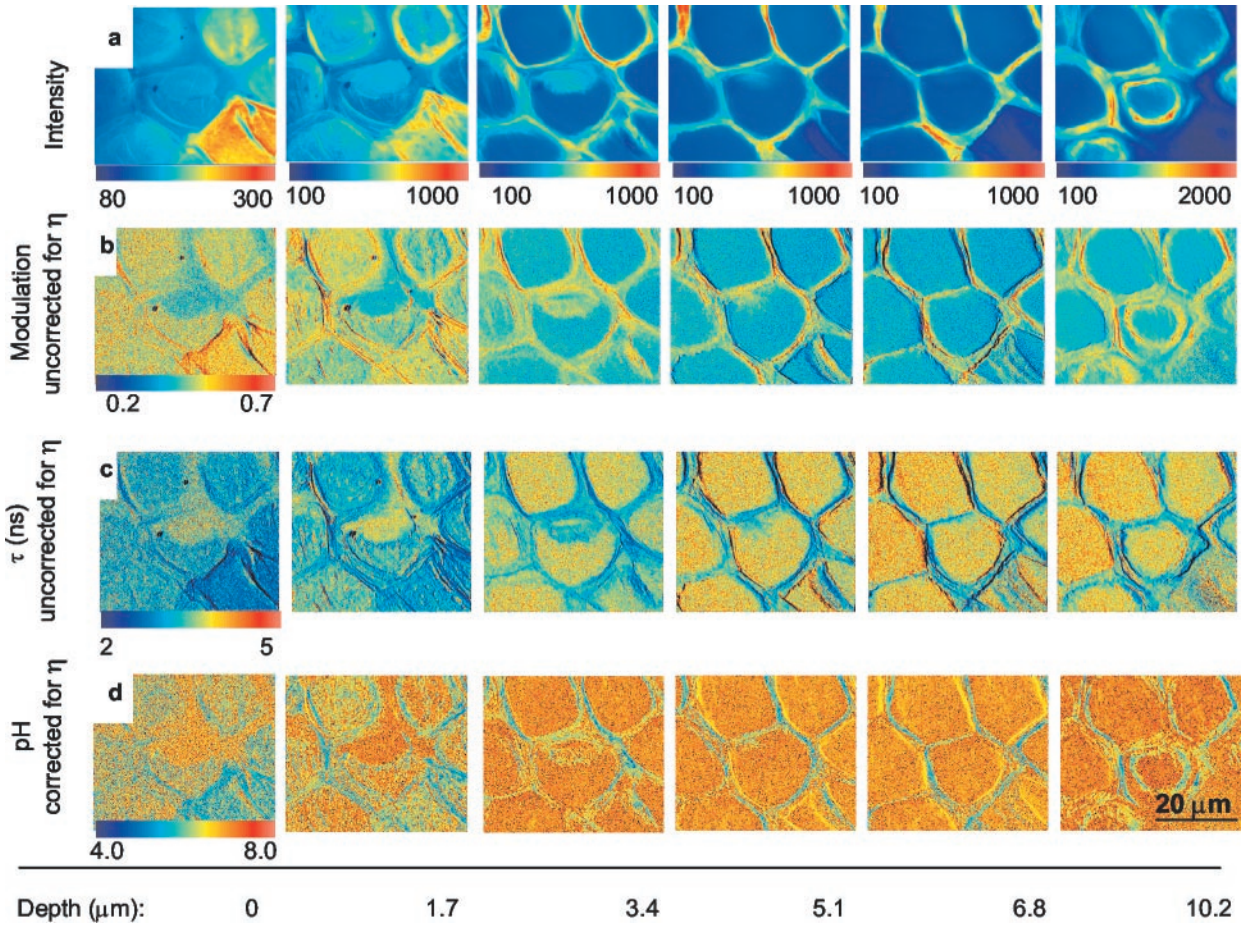

FIGURE 4 Intensity (*a*), modulation (*b*), and lifetime (τ) (*c*) images and pH maps (*d*) of hairless mouse skin (Crl:SKH1-hrBR) at different epidermal depths. As the intensity images show, BCECF distributed unevenly because of the barrier nature of the stratum corneum, making direct pH measurements based on fluorescence intensity impossible. The pH maps indicate acidic regions (average pH 6.0) within the extracellular matrix of the stratum corneum. Except for the corneocytes sloughing off from the surface, intracellular pH is near neutral (average pH 6.7).

Therefore, we consider the effect of refractive index (η) of the environment surrounding the fluorophore on lifetime data. The fluorescence lifetime τ is described by

$$\tau = (\Gamma = k_{nr})^{-1}, \tag{14}$$

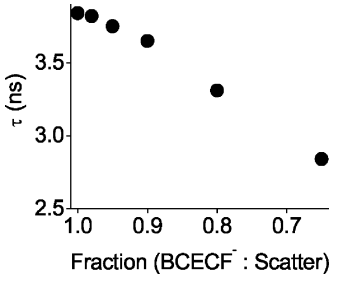

FIGURE 5 The effect of autofluorescence and/or scatter upon τ of BCECF. Increasing background increases the detected modulation value. Background from our samples contributed <1% to the overall intensity measured.

where Γ is the rate of radiative decay and k_{nr} is the nonradiative rate constant (from all sources). The Strickler-Berg equation shows that Γ is dependent upon η and the extinction coefficient ϵ at frequency ν (cm^{-1}) where ν_o is equivalent to the frequency of the ground-state to first singlet-state transition:

$$\Gamma = 2.88 \times 10^{-9}\eta^2 \int \frac{(2\nu_0 - \nu)^2}{\nu}\,\varepsilon_\nu d\nu \tag{15}$$

Assuming that the viscosity, which affects k_{nr}, is similar between environments, then to a first approximation we can assume that only η affects τ (Ephardt and Fromherz, 1989; Fushimi and Verkman, 1991; Luby-Phelps et al., 1993). Thus,

$$\tau \propto \eta^{-2} \tag{16}$$

To determine the effect of different indices of refraction of skin and solution on τ, we compared fluorescence life-

TABLE 2 Lifetime and refractive index data of BCECF and fluorescein

	τ_{BCECF^-} (ns)	η
BCECF pH 7.1 solution	3.87	1.33
BCECF in stratum granulosum and deeper layers	3.63	1.37*
Fluorescein pH 7.1 solution	4.05	1.33
Fluorescein in stratum granulosum and deeper layers	3.73	1.39*

*Calculated using $\frac{\tau_{skin}}{\tau_{solution}} \propto \frac{(\eta_{solution})^2}{(\eta_{skin})^2}$

time imaging (FLIM) measurements in aqueous solution ($\eta_{water} = 1.33$) and mouse skin. These comparisons were carried out with both fluorescein, whose lifetime does not alter with pH, and lifetime-sensitive BCECF. Table 2 lists the lifetime values for the two fluorophores at pH 7.2 and in the mouse stratum granulosum (pH 7 (Dikstein and Zlotogorski, 1994; Ohman and Vahlquist, 1994, 1998)). For both fluorophores, the τ is 1.1 times less in the skin's viable (pH 7) epidermal layers than in the pH 7 solution. Using Eq. 16 and the values in Table 2, we calculate η_{skin}, (1.37–1.39); this is in excellent agreement with previous measurements of η in the stratum granulosum ($\eta = 1.36$–1.43, (Knuttel and Boehlau-Godau, 2000)).

The stratum corneum is only 15% water and is composed of a network of lipid-rich extracellular matrix and protein-rich intracellular space. Therefore, we can assume that η does not vary dramatically between environments of the skin (Schaefer and Redelmeier, 1996; Krishna and Persiasamy, 1998). The differences between the τ values in solution in the range of pH 5.6 to 7.5 are similar to the differences in τ values between surface (average pH 6) and viable strata (pH 7) of mouse skin. The lifetime increases 1.2 times between the mouse skin surface and the stratum granulosum (Fig. 3 *d*). The lifetime remains constant with increasing depth below the corneocytes in all viable strata of mouse skin (Fig. 3 *d*). In solution, a similar difference (1.2-fold decrease) in the lifetime is detected between approximately pH 6 BCECF and pH 7 BCECF (Fig. 3 *c*). This is identical to the reported pH difference between the cornified and granular strata of mouse skin (Dikstein and Zlotogorski, 1994; Ohman and Vahlquist, 1994). We would anticipate that if η varied dramatically between stratum corneum depths and microenvironments, then correction of the skin τ values using one η value would lead to pH values that were not within the pH range anticipated by tape-stripping measurements. Thus, we conclude that the refractive index does not dramatically change with each increasing epidermal depth or between microenvironments within the stratum corneum.

Because η of the surrounding environment affects the corresponding lifetime-resolved data of the fluorophore, the phase and modulation values of BCECF acquired in the skin

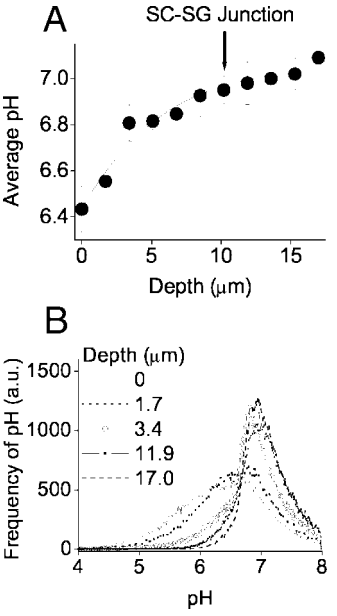

FIGURE 6 pH data of the stratum corneum. (*a*) Average pH as a function of depth. Each data point represents the average of the pH maps ($\leq 50 \times 50$ μm) taken from two different mouse skin samples. (*b*) Histograms of pH at different epidermal depths. The histogram data shows more clearly than *a* that two pH values are prevalent in the stratum corneum. With increasing depth, the frequency of acidic pH readings decreases. *b* indicates that the average pH in *a* increases with depth because of a decrease in the number of acidic regions contributing to the overall pH value.

are corrected for η at each pixel (see Materials and Methods). Consequently, this adjustment accounts correctly for the species fractions of HBCECF and $BCECF^-$. Because this correction can be determined at each point, the pH can be calculated (Eq. 13) accurately.

Calculating pH at each depth

Fig. 4 *c* displays pH maps of hairless mouse skin as a function of stratum corneum depth. The pH at each pixel is calculated from lifetime-resolved data that has been corrected for the difference in η between BCECF in solution and BCECF in skin. Fig. 6 *a* shows that the average pH of each image (calculated over the entire image area at each depth) gradually increases with depth, which is consistent with tape-stripping measurements (Ohman and Vahlquist, 1994, 1998). The surface pH of animals, including mice, is less acidic than that of humans and thus gives rise to a smaller change in pH over its stratum corneum (Dikstein and Zlotogorski, 1994). Tape-stripping measurements cannot distinguish spatially distributed pH values. Our pH maps identify regions of higher and lower pH within each image at different stratum corneum depths. BCECF is often used as a probe to detect intracellular pH (Haughland, 1998). The intensity images (Fig. 4 *a*) show that BCECF

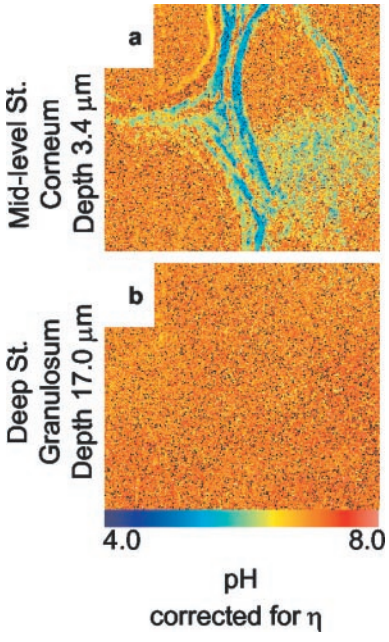

FIGURE 7 Magnified images of pH (25 × 25 μm) of stratum corneum and deep stratum granulosum layers.

concentrates in both the lipid-rich matrix and intracellular spaces of the keratinocytes. The minimum fluorescence intensity of the intracellular spaces is 100 counts, which is significantly above autofluorescence (<4 counts). This characteristic makes BCECF a useful dye for determining pH in both areas of the stratum corneum. We emphasize that the lipid matrix of the stratum corneum is not entirely lipid and is described as having aqueous microdomains. The water content of the extracellular matrix of the stratum corneum is between 2 and 200 mM (Schaefer and Redelmeier, 1996).

A corneocyte (~25 μm diameter) that appears to be sloughing off the surface is highly acidic (Fig. 4 *a*). There are pockets (~1 μm diameter) throughout the stratum corneum in the extracellular matrix where the pH is lowest (average pH 6.0). However, the intracellular pH of the corneocytes remains more neutral (average pH 6.7). Images representative of the extracellular acidic pockets and neutral viable layers are displayed in Fig. 7. The magnified image of the stratum corneum clearly shows that the lipid matrix itself is not entirely acidic. Acidic pockets within the matrix account for the acidity detected.

A histogram of the pH at the stratum corneum surface shows that regions with pH 6.0 contribute largely to the structural make-up of the stratum corneum surface (Fig. 6 *b*). The number of areas with pH 6.0 gradually decreases with the depth of focus until the stratum granulosum is reached (Fig. 6 *b*). At this point, areas with pH 6.0 are almost absent. Instead, the average pH is 7.0. This agrees with the average pH value detected by tape-stripping measurements on human and mouse skin (Ohman and Vahlquist, 1994).

The pH maps and histogram data definitively prove that the pH of the stratum corneum does not increase because of a uniform increase in pH with depth. The images show that the average pH of the extracellular regions of mouse skin remains essentially constant at pH 6.0 at all depths. The histogram data clearly indicate that the average pH of the skin increases with each successive stratum corneum layer because of a decrease in the number of acidic extracellular regions contributing to the overall pH value. The lowest pH value and largest number of acidic regions are detected at the stratum corneum surface where corneocytes, which are acidic, are sloughing off. The highest pH (which is neutral) is achieved in the viable epidermis, which has an absence of extracellular ceramide-rich lipid matrix found in the stratum corneum (Fig. 7).

CONCLUSIONS

Two-photon fluorescence lifetime-resolved imaging microscopy was selected because it affords submicron spatial resolution and submillimeter depth penetration into tissue using one excitation wavelength. This technique provides an excellent method for imaging cellular processes on the submicron scale within all layers of the epidermis.

The primary issue in determining pH in the skin accurately has been one of calibration (Hanson et al., 2000). Lifetime imaging circumvents this difficulty because lifetime measurements are independent of concentration, which allows for a straightforward calibration. Intensity measurements are difficult to calibrate because the pH-sensitive dyes are unevenly distributed. This is because of the heterogeneous environment and efficient barrier properties of the stratum corneum. As Fig. 4 *a* shows, a region of bright intensity may indicate either a neutral pH or simply the presence of a greater number of dye molecules relative to another area within the skin. Ratiometric measurement techniques can circumvent the issue of uneven dye distribution. The dye, BCECF, that we have used in our lifetime-resolved experiments, has been used to detect intracellular pH differences using intensity excitation-ratio measurements (Rink et al., 1982). Because the excitation spectrum of BCECF spectrally shifts with pH, a fluorescence emission intensity ratio can be formed by exciting at two wavelengths. However, this is experimentally inconvenient; with two-photon FLIM only one excitation wavelength is needed. This avoids the movement of the excitation beam within the focal plane that results when excitation wavelengths are changed, which is a serious problem in ratiometric methods. The ratiometric measurements have also proven to be difficult to calibrate within the skin (Turner et al., 1998). However, with the development of new probes that spectrally shift over the entire pH range of the stratum

corneum, emission ratio imaging of stratum corneum pH may prove comparable in ease of use to two-photon FLIM.

Several mechanistic theories have been published to explain the origin of the stratum corneum acid mantle. Passive mechanisms proposed to date include the accumulation of the ultraviolet chromophore *trans*-urocanic acid (Krien and Kermici, 2000), sweat by-products lactate and lactic acid (Patterson et al., 2000), or acidic free fatty acids (Lieckfeldt et al., 2000). These mechanisms differ from active pathways (sodium/hydrogen antiporter) that may influence pH by actively regulating the hydrogen ion concentration. We are currently using two-photon FLIM to determine the effect of active and passive mechanisms upon the origin of acidic microdomains within the stratum corneum.

The Laboratory for Fluorescence Dynamics at the University of Illinois is supported by National Institutes of Health PHS P41-RR03155. K.H. is supported by the Cancer Research Foundation of America and the Skin Cancer Foundation.

REFERENCES

Alcala, J. R., E. Gratton, and D. M. Jameson. 1985. A multifrequency phase fluorometer using the harmonic content of a mode-locked laser. *Anal. Instr.* 14:225–250.

Christophers, E. 1971. Cellular architecture of the stratum corneum. *J. Invest. Dermatol.* 56:165–169.

Clegg, R. M., and P. C. Schneider. 1996. Fluorescence lifetime-resolved imaging microscopy: a general description of lifetime-resolved imaging measurements. *In* Fluorescence Microscopy and Fluorescent Probes. J. Savik, editor. Plenum Press, New York. 15–33.

Dikstein, S., and A. Zlotogorski. 1994. Measurement of skin pH. *Acta Dermatol. Venereol.* (*Stockh.).* 185:18–20.

Ephardt, H., and P. J. Fromherz. 1989. Fluorescence and photoisomerization of an amphiphilic aminostilbazolium dye as controlled by the sensitivity of radiationless deactivation to polarity and viscosity *J. Phys. Chem.* 93:7717–7725.

Fushimi, K., and A. S. Verkman. 1991. Low viscosity in the aqueous domain of cell cytoplasm measured by picosecond polarization microfluorimetry. *J. Cell Biol.* 112:719–725.

Hanson, K. M., N. P. Barry, E. Gratton, and R. M. Clegg. 2000. Fluorescence lifetime imaging of pH in the stratum corneum. *Biophys. J. Annu. Meet. Abstr.* B588.

Haughland, R. P. 1998. Handbook of Fluorescent Probes and Research Chemicals. T. Z. Spence, editor. Molecular Probes, Eugene, OR.

Jacques S. L. 1996. Modeling light propagation in tissues. *In* Biomedical Optical Instrumentation and Laser-Assisted Biotechnology. A. M. Verga Scheggi, editor. Kluwer Academic Publishers, Amsterdam. 21–32.

Jameson, D. M., E. Gratton, and R. D. Hall. 1984. The measurement and analysis of heterogeneous emissions by multifrequency phase and modulation fluorometry. *Appl. Spectrosc. Rev.* 20:55–106.

Knuttel, A., and M. Boehlau-Godau. 2000. Spatially confined and temporally resolved refractive index and scattering evaluation in human skin performed with optical coherence tomography. *J. Biomed. Optics.* 5:83–92.

Krien, P. M., and M. Kermici. 2000. Evidence for the existence of a self-regulated enzymatic process within the human stratum corneum: an unexpected role for urocanic acid. *J. Invest. Dermatol.* 115:414–20.

Lakowicz, J. R. 1999. Principles of Fluorescence Spectroscopy. Kluwer/Plenum, New York.

Lieckfeldt, R., J. Villalain, J. C. Gomez-Fernandez, and G. Lee. 1995. Apparent pKa of the fatty acids within ordered mixtures of model human stratum corneum lipids. *Pharmacol. Res.* 12:1614–7.

Luby-Phelps, K., S. Mujumdar, R. Mujumdar, L. Ernst, W. Galbraith, and A. Waggoner. 1993. A novel fluorescence ratiometric method confirms the low solvent viscosity of the cytoplasm. *Biophys. J.* 65:236–242.

MacKenzie, I. C. 1969. Ordered structure of the stratum corneum of mammalian skin. *Nature.* 222:881.

Masters, B. R., P. T. C. So, and E. Gratton. 1997. Multiphoton excitation fluorescence microscopy and spectroscopy of in vivo human skin. *Biophys. J.* 72:2405–2412.

Ohman, H., and A. Vahlquist. 1994. In vivo studies concerning a pH gradient in human stratum corneum and upper epidermis. *Acta Dermatol. Venereol.* (*Stockh.).* 74:375–379.

Ohman, H., and A. Vahlquist. 1998. The pH gradient over the stratum corneum differs in X-linked recessive and autosomal dominant icthyosis: a clue to the molecular origin of the acid skin mantle. *J. Invest. Dermatol.* 111:674–677.

Patterson, M. J., S. D. Galloway, and M. A. Nimmo. 2000. Variations in regional sweat composition in normal human males. *Exp. Physiol.* 85: 869–875.

Rink, T. J., R. Y. Tsien, and T. Pozzan. 1982. Cytoplasmic pH and free Mg^{2+} in lymphocytes. *J. Cell Biol.* 95:189–196.

Schaefer, H., and T. E. Redelmeier. 1996. Skin Barrier: Principles of Percutaneous Absorption. Karger, Basel, Switzerland. 48–49.

So, P. T. C., T. French, W. M. Yu, K. M. Berland, C. Y. Dong, and E. Gratton. 1996. Two photon fluorescence microscopy: time-resolved and intensity imaging. *In* Fluorescence Imaging and Microscopy. X. F. Wang and B. Herman, editors. John Wiley and Sons, New York. 51–374.

Szmacinski, H., and J. R. Lakowicz. 1993. Optical measurements of pH using fluorescence lifetimes and phase-modulation fluorometry. *Anal. Chem.* 65:1668–1674.

Turner, N. G., C. Cullander, and R. H. Guy. 1998. Determination of the pH gradient across the stratum corneum. *J. Invest. Dermatol. Symp. Proc.* 3:110–113.